CHEMISTRY OF MATERIALS

pubs.acs.org/cm

Article

High Activity toward the Hydrogen Evolution Reaction on the Edges of MoS_2-Supported Platinum Nanoclusters Using Cluster Expansion and Electrochemical Modeling

Timothy T. Yang, Teck Leong Tan, and Wissam A. Saidi*

Cite This: *Chem. Mater.* 2020, 32, 1315−1321

Read Online

ACCESS | Metrics & More | Article Recommendations | Supporting Information

ABSTRACT: The design of efficient and cost-effective platinum-based catalysts for the hydrogen evolution reaction (HER) is critical for energy sustainability. Herein, we report high catalytic activity toward HER on the edges of platinum nanoclusters (NCs) supported on single-layer molybdenum disulfide and provide a direct link between ab initio calculations and electrochemical experiments. We determine the active catalytic sites using a cluster expansion method in conjunction with an ab initio thermodynamic approach and show that the system is thermodynamically active at HER reversible potential under electrochemical conditions. We also show that the preferred HER mechanism is the Volmer−Tafel pathway with the Volmer reaction as the rate-determining step. Using a Butler−Volmer kinetic model to simulate a linear sweep voltammogram, we obtain an exchange current density of 10^{-3}−10^{-2} A/cm^2, which is in the same order as those measured for Pt(111) and supported Pt NCs. Importantly, we show that, contrary to expectations, the enhanced HER mechanism is only attributable to the edges of the supported Pt NCs but not due to metal−support interactions. Our findings are general and applicable to NCs with different sizes and shapes on various supports as well as to different catalytic reactions.

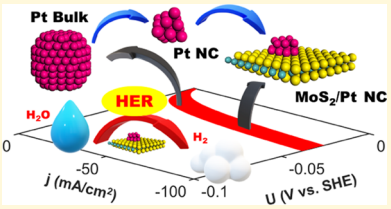

Downloaded via UNIV OF PITTSBURGH on July 14, 2020 at 00:30:51 (UTC).
See https://pubs.acs.org/sharingguidelines for options on how to legitimately share published articles.

INTRODUCTION

The diminishing supply of fossil fuels and pollution problems associated with combustion reactions led to the search for sustainable and environmentally benign energy sources. Hydrogen is one of the potential alternatives that can be produced via the hydrogen evolution reaction (HER), a critical reaction of water electrolysis by splitting water using electrical energy from solar or wind power.[1] While platinum (Pt) is the most efficient catalyst for HER, its relatively high cost limits its commercial applications.[2] This explains the huge interest in reducing the content of Pt in HER electrodes or in finding cost-effective and equally efficient alternative catalysts.[3−5]

Platinum nanoclusters (NCs) offer a very attractive route to reduce Pt usage.[6,7] Pt NCs are tiny building blocks of matter containing a finite number of Pt atoms, which are often attached to substrates to prevent agglomeration. In contrast to bulk counterparts, the efficiency of metallic NC catalysts can be tuned by modifying their morphology or supports. For example, Anderson et al. demonstrated that the size of Pt NCs affects oxygen reduction and carbon oxidation;[8] Nakajima et al. showed that HER activity can be maximized for a certain size of Pt NCs.[9] Recently, Huang et al. found that supported Pt NCs on MoS_2 exhibit superior catalytic activity toward HER, which is comparable to that of bulk Pt despite an ∼70% reduction in the Pt content.[10] However, the atomistic HER mechanism of supported Pt NCs on MoS_2 is lacking, thus hampering further improvements and optimizations of the catalysts.

There are several challenges associated with the understanding of the HER mechanism of supported or even unsupported metal particles. For Pt bulk systems, the HER mechanism is easily determined as their active sites are mostly identical on a well-defined surface.[11] In addition, the most exposed surfaces (111) and (100)[12,13] exhibit similar HER rates, as evidenced by less than 1 order of magnitude difference in exchange currents.[14,15] However, different from the bulk counterparts,[11,16] NCs are rich in edges and vertices, which show a variety of active sites that dominate HER activity over facets.[17,18] Additionally, supporting substrates of the NCs can also influence the HER activity either through exposing edge sites or modifying charges in the basal plane[19] or due to a concerted interplay between the supports and NCs.[20]

Experimentally, it is also challenging to infer the HER mechanism using conventional electrochemical analysis. First, most of the experimental methods can only provide an ensemble assessment over different active sites.[21] For example, previous studies have shown that the HER activity on either Pt atoms or Pt clusters cannot be distinguished.[7,21,22] Second, HER rates for high catalytic activity systems such as Pt are relatively fast, which results in the depletion of reactants near the electrode surface. The concentration gradients in both

Received: December 18, 2019
Revised: January 3, 2020
Published: January 7, 2020

ACS Publications

© 2020 American Chemical Society

https://dx.doi.org/10.1021/acs.chemmater.9b05244
Chem. Mater. 2020, 32, 1315−1321

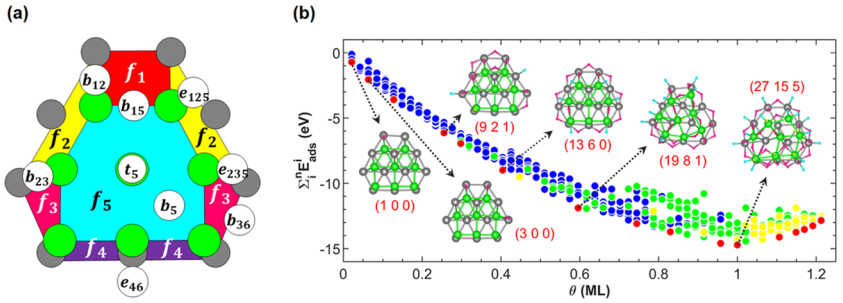

Figure 1. (a) Schematic of MoS_2/Pt_{20} and hydrogen adsorption sites. Facets of the supported Pt_{20} labeled as f_i (i = 1−4) correspond to the sides of the cluster. f_5 and f_6 (not shown) are the top and the bottom facets, respectively. A few adsorption sites are labeled as white spheres, while the Pt atoms at the top/bottom layer are represented by green/gray spheres. (b) Total adsorption energy, $\sum_i^n E_{ads}^i$, for different adsorption configurations on MoS_2/Pt_{20}. The most stable configurations are indicated by the red dots. The distortion of the supported Pt_{20} is measured by the displacement of top Pt atoms for less than 0.5, between 0.5 and 1, and above 1 Å/atom that are represented by blue, green, and yellow dots, respectively. The number of adsorbed hydrogen atoms at bridge, corner, and top sites, which are represented respectively by magenta, blue, and yellow spheres in the insets, are shown as triplets in parentheses.

oxidants and reactants make hydrogen mass transport the dominant rate for HER. Sheng et al. argued that such a limitation cannot be avoided using conventional rotating electrodes.[23] Additionally, the impendence from the electrolyte can also affect current measurements on fast HER electrodes even with highly conductive electrolytes such as 0.1 M $HClO_4$.[24]

First-principles calculations are attractive alternatives to experiments that provide atomistic descriptions of active sites and mechanisms of Pt systems. However, in comparison to surfaces and periodic systems, supported metal clusters pose a significant challenge in simulation due to the combination of periodic (supports) and nonperiodic (Pt NCs) elements in the hybrid systems. Thus, it is computationally daunting to find equilibrium NC morphologies as well as optimum hydrogen adsorption configurations on nonequivalent adsorption sites of supported metal clusters[25] under electrochemical conditions.

Herein, we investigate the HER activity of supported Pt NCs on MoS_2 with a relatively small number of Pt atoms that cannot be modeled using a periodic slab approach. We use first-principles density functional theory (DFT) calculations in conjunction with a cluster expansion method and an ab initio thermodynamic approach to determine HER catalytic sites. Electrochemical modeling is then used to quantify the exchange current and simulate the linear sweep voltammogram. Our main finding is that the HER current from the supported Pt NCs is comparable to that from Pt(111) due to the cluster's catalytic edge sites. In addition, we show the metal−support interactions do not affect the HER mechanism and catalytic activity. This finding agrees with experimental results, which reported that supported Pt NCs on MoS_2 have a comparable efficiency to that of bulk Pt.[10] However, our computed current is higher than the experimental values in ref 10 but is in good agreement with that of Pt nanoparticles on a carbon support.[22,26] We argue that such a discrepancy with the results in ref 10 is due to the limitation of diffusion and electrode impedance that were not accounted for in standard electrochemical measurements.

METHODOLOGY

We use the CP2K[27] for first-principles density functional theory (DFT) calculations employing revised Perdew−Burke−Ernzerhof exchange−correlational functional to solve the Kohn−Sham equations.[28] More details are given in the Supporting Information (SI). Previously, we employed a self-consistent, combined theoretical and experimental approach to determine atom-by-atom the structures of supported Pt NCs on MoS_2 with up to 38 Pt atoms. The atomic structures are predicted using a genetic algorithm utilizing adaptive atomistic force fields and DFT, which are then validated using aberration-corrected scanning transmission electron microscopy.[29] Herein, we investigate MoS_2/Pt_{20} as a representative of a supported Pt NC on MoS_2 but we argue later that our findings are general and applicable to other NCs with different morphologies. Pt_{20} is ∼1 nm in diameter, 12 atoms are in the bottom layer that is in contact with MoS_2, and 8 Pt atoms are in the top layer with an average Pt−Pt distance of 2.7 ± 0.2 Å, in agreement with experimental high-resolution transmission electron microscopy (HRTEM) analysis.[10,29] To evaluate hydrogen stability, we define the adsorption energy as

$$E_{ads}^{n} = E_{(n+1)H^*} - E_{nH^*} - 0.5E_{H_2} \quad (1)$$

where $E_{(n+1)H^*}$ and E_{nH^*} are the DFT energies of the system with n + 1 and n adsorbed hydrogen H* and E_{H_2} is the DFT energy of H_2 in the gas phase.

We use a cluster expansion (CE) method, as implemented in the TTK code package,[30,31] to model the effective interactions between H* at different coverages. We identify symmetry-unique adsorption sites including hollow, bridge, corner, and atop sites. For each site, k, we assign an occupation variable ξ_k with the value of 1(0) to represent a site occupied (unoccupied) by H*.[16] For a particular configuration σ arranged by small hydrogen clusters α, the cluster expansion energy is written as

$$E_{CE}(\sigma) = \sum_{\alpha} V_\alpha \phi_\alpha \text{ with } \phi_\alpha = \prod_{k\in\alpha} \xi_k \quad (2)$$

where V_α is the effective cluster interaction (ECI). In practice, a properly truncated Hamiltonian will predict the energies accurately as V_α is close to zero with increasing distances between H*. Only the symmetrical ECIs in the truncated Hamiltonian are evaluated from a finite set of DFT configuration energies as the training set. In an initial iteration, random distributions of H* with their energies $E_{CE}(\sigma)$ are obtained via Monte Carlo sampling across different coverages as well as the optimal ECIs. Another round of Monte Carlo sampling is required to obtain new low-energy structures to compare with DFT structures. The DFT-verified structures are

https://dx.doi.org/10.1021/acs.chemmater.9b05244
Chem. Mater. 2020, 32, 1315−1321

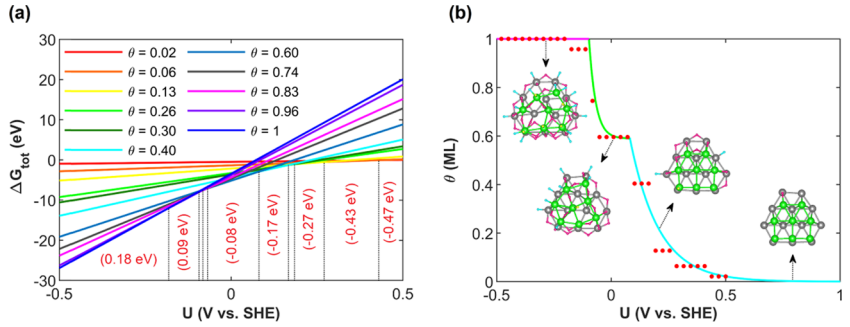

Figure 2. (a) Thermodynamic isotherm constructed using eq 4. At a given potential, the lowest line indicates the corresponding hydrogen coverage. The corresponding ΔG_H values for each θ are shown in parentheses. (b) θ as a function of U extracted from (a). The inset shows the low-energy hydrogen configurations at different U's.

then added to the training set for a subsequent round of cluster expansion except for highly distorted structures at high coverages. This process is repeated 3 times for finding low-energy hydrogen adsorption configurations until no new low-energy configurations are suggested by the Monte Carlo simulations. We note that structural relaxations for Pt and H atoms are allowed during DFT calculations. Because water has only a small effect on hydrogen adsorption energies (see the SI), it is excluded for determining H* configurations using the cluster expansion method.

RESULTS

Hydrogen mainly interacts with Pt NC but not with the MoS_2 support.[32,33] Figure 1a shows a schematic of the supported Pt cluster with three main hydrogen adsorption sites, namely, the atop sites (t) of Pt atoms, the bridge (b) sites in between two Pt atoms, and the edge (e) sites associated near Pt atoms at the edges of the cluster. The strongest adsorption is at the bridge sites b_{12} ($-0.71 < E^1_{ads} < -0.68$ eV) located at the edges of side facets f_1 and f_2, while the weakest sites are the atop sites t_{45} ($-0.15 < E^1_{ads} < -0.10$ eV) of the corner Pt at the edges of f_4 and f_5. The other strong adsorption sites are the bridge sites b_{i5}/b_{i6} ($-0.60 < E^1_{ads} < -0.47$ eV) at the top/bottom layer f_5/f_6 and the edges/corners of two/three facets such as e_{i5}, e_{i6}/e_{ij5}, and e_{ij6} ($-0.45 < E^1_{ads} < -0.28$ eV), for any i and j with $i \neq$ j. There are a few moderate adsorption sites such as the bridge sites on top of the Pt cluster, b_5, and the top site at Pt terrace, t_5 ($-0.38 < E^1_{ads} < -0.26$ eV). Furthermore, the adsorption strength is also found to be sensitive to the Pt cluster's local topology as identified by microfacets f_i. We find that the adsorption strength near f_4 is relatively weaker, while it is stronger near f_1.

We have trained a CE effective Hamiltonian using 400 different configurations with up to 57 adsorbed hydrogen atoms distributed among 47 adsorption sites on the Pt NC. Figure 1b shows the total hydrogen adsorption energy, $\sum_i^n E^i_{ads}$, for the configurations with n = 1, 2, ⋯ 57. For each n, we identify the low-energy configurations with the lowest $\sum_i^n E^i_{ads}$ as indicated by red dots.[16] The inset in the figure depicts a few of these low-energy configurations. The hydrogen coverage θ = 1 corresponds to n = 47 at which $\sum_i^n E^i_{ads}$ has the lowest value among all n. This indicates that the adsorption sites on the NC are fully occupied. The definition of full occupation is chosen to be consistent with periodic metal surfaces that undergo a sharp weakening of hydrogen adsorption strength right above θ = 1.[34] As θ increases, the top layer of the Pt NC distorts to a less symmetrical form, while the bottom layer remains relatively intact due to its strong affinity with MoS_2.[35]

Hydrogen adsorption strength is highly affected by adsorption configurations due to adsorbate−adsorbate and adsorbate−surface interactions. In agreement with our previous findings on β-Mo_2C surfaces with nonequivalent adsorption sites,[36] we show that the filling sequence follows the adsorption strength of single H* as shown in Figure 1b; b_{12}, b_{23}, and b_{15} are occupied starting at θ = 0.06, followed by b_{i5}, b_{i6}, e_{i5}, e_{i6}, e_{ij5}, and e_{ij6} up to θ = 0.4. Moderate adsorption sites, b_5, are filled at θ = 0.6 followed by t_5 up to θ = 1.

DISCUSSION

Hydrogen evolution reaction $2H^+ + 2e^- \rightarrow H_2(g)$ is the formation of hydrogen gas $H_2(g)$ from hydrogen ions. Parsons argued that the HER rate is related to atomic hydrogen adsorption ability on the surface,[2] which was quantified by Nørskov using the hydrogen adsorption free energy, ΔG_H, from first-principles calculations defined as[25]

$$\Delta G_H = E^n_{ads} + \Delta E_{ZPE} - T\Delta S \quad (3)$$

where E^n_{ads} is defined by eq 1 and ΔE_{ZPE} and ΔS are respectively the differences of zero-point energy and entropy between H* and $H_2(g)$. Using experimental thermodynamic results for $H_2(g)$, we determine $T\Delta S$ to be −0.2 eV at room temperature when assuming the entropy of adsorbed hydrogen to be approximately zero.[37] We obtain $\Delta E_{ZPE} \sim 0.04$ eV, which is similar to that of Pt(111) and other metal surfaces.[25] For ΔG_H = 0, HER achieves optimum activity as hydrogen interacts neither too strongly nor too weakly with the catalytic surface. Away from ΔG_H = 0, the HER activity decreases as hydrogen in the adsorbed state (gas state) is more favored than that in the gas state (adsorbed state) for $\Delta G_H < 0$ ($\Delta G_H > 0$).

Figure 2a shows the hydrogen adsorption isotherm obtained from evaluating the total adsorption free energy

$$\Delta G_{tot} = \sum_i^n \Delta G_H - nle|\eta \quad (4)$$

where $\eta = U - U_{SHE}$ is the overpotential.[13,38] For an applied external potential, U, with respect to the standard hydrogen potential U_{SHE}, the most stable coverage has the lowest value of ΔG_{tot}. Coverages at different potentials are summarized in Figure 2b. As seen in the figure, hydrogen coverage is nearly zero above 0.5 V vs SHE. At 0 V vs SHE where HER is reversible, the HER activity approaches to optimum indicated by ΔG_H = −0.08 eV, which is in line with a previous study[11] showing ΔG_H = 0 eV for Pt(111). Meanwhile, the corner and

https://dx.doi.org/10.1021/acs.chemmater.9b05244
Chem. Mater. 2020, 32, 1315−1321

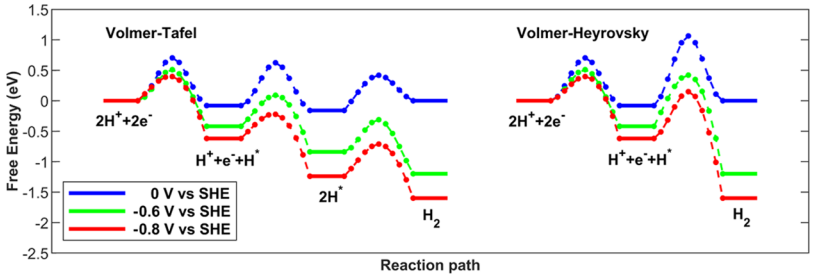

Figure 3. Reaction pathways at three selected overpotentials. Solid horizontal lines represent the reaction free energies calculated from eq 5, and dashed curves represent reaction paths with kinetic barrier, E_k, at the peaks.

edge sites are mainly occupied, whereas the site on top of the NC remains empty, as shown in Figure 1b. This draws an important conclusion that the high HER activity is due to the edges of the Pt NCs.

In acidic solutions, there are two HER pathways, namely, the Volmer–Tafel and Volmer–Heyrovsky with the elementary reactions as

$$H_3O^+ + e^- \rightarrow H^* + H_2O \quad \text{(Volmer)}$$

$$H_3O^+ + e^- + H^* \rightarrow H_2O + H_2 \quad \text{(Heyrovsky)}$$

$$H^* + H^* \rightarrow H_2 \quad \text{(Tafel)}$$

The corresponding reaction free energies of the three elementary steps can be written as (see detailed derivation in the SI)

$$\delta G = \begin{cases} \Delta G_H + e\eta & \text{(Volmer)} \\ -\Delta G_H + e\eta & \text{(Heyrovsky)} \\ -2\Delta G_H. & \text{(Tafel)} \end{cases} \quad (5)$$

To mechanistically understand the HER kinetics on MoS_2/Pt_{20} and quantify the HER rate in an acidic electrochemical environment, we determine the minimum energy pathways for the three elementary reactions using a standard setup for the solid–liquid interface (see SI).[39] We focus at θ = 0.6 and 1, which are the equilibrium coverages under 0 V and below −0.2 V, as shown in Figure 2. For the Volmer and Heyrovsky reactions, we investigate several reaction sites focusing mainly on t_5 and b_5. For the Tafel reaction, we test several combinations on t and b sites. In the real electrochemical solid–water interface, the potential across the Helmholtz layer does not change during redox reactions, while it is not the case for finite-size solid–water interface models. To correct for this finite-size supercell effect, we use an extrapolation scheme that was recently employed for HER on the Pt(111) surface (see the SI).[40]

Figure 3 shows the HER minimum energy pathways on MoS_2/Pt_{20} at three different applied potentials 0, −0.6, and −0.8 V. The reaction free energy, δG, obtained from eq 5 is indicated by horizontal lines, and the kinetic barrier, E_k, is indicated by the peaks of the curves. We show that the HER mechanism is mainly dictated by the kinetic barrier as δG either decreases or increases only slightly along the pathways. At 0 V vs SHE, the kinetic barrier 1.1 eV of the Heyrovsky reaction is the highest, followed by the Volmer 0.7 eV, while the Tafel 0.6 eV is the lowest. Thus, the HER follows the Volmer–Tafel pathway with the Volmer as the rate-determining step (rds). This pathway remains unchanged until the applied voltage decreases to −0.6 V. At −0.8 V, the barrier of the Volmer reaction decreases below that of the Tafel reaction; thus, the rds for the preferred Volmer–Tafel pathway becomes the Tafel reaction. As the kinetic barrier of redox reactions (the Volmer and the Heyrovsky) decreases with increasing negatively applied potential, and as the barrier of the Tafel reaction is independent of η, we expect that the Volmer–Heyrovsky route will eventually become the preferred reaction pathway at a sufficiently large applied overpotential below −0.8 V. Our result is consistent with bulk Pt where the contributions of the Volmer–Tafel and the Volmer–Heyrovsky pathway to the HER current are found to be potential-dependent.[41] Further discussions on the comparison between the HER reactions on MoS_2/Pt_{20} and the periodic Pt(111) system are given in the SI. While the investigation of the HER pathways on all of the possible active sites is not exhaustive, we do not expect the mechanism as well as the kinetic barrier results to be appreciably underestimated given that H* diffusion on the cluster is fast with barriers less than 0.1 eV (see the SI).

The Butler–Volmer relation is commonly used to study the HER on Pt catalysts,[22,23,42−44] which describes the total Faradaic current, j, as the sum of cathodic $j_0 e^{-\alpha f\eta}$ and anodic $j_0 e^{(1-\alpha)f\eta}$ currents

$$j = j_0\left(e^{-\alpha f\eta} - e^{(1-\alpha)f\eta}\right) \quad (6)$$

Here, $f = F/k_BT$ with F being the Faraday constant and k_B being the Boltzmann constant. α is the transfer coefficient that implicitly describes charge-transfer kinetics from the water layer to the electrode surface between the initial and transition states. Experimentally, α is determined to be 0.5 for Pt NCs.[22] The exchange current density, j_0, for the Volmer reaction as the rds can be written as

$$j_0 = nFC_{tot}(1-\theta)\frac{k_BT}{h}\exp\left(-\frac{E_k}{k_BT}\right) \quad (7)$$

where C_{tot} is the total concentration of H^+ and H* near the electrode surface. Thus, we can define $nFC_{tot} = eN_{site}/A$, where N_{site} is the number of active sites on the surface with area A. The energy barrier, E_k, corresponds to the rds (Volmer reaction) determined at zero potential. Using the upper (lower) limit of E_k = 0.79 eV (0.70 eV) to account for the variations in kinetic barriers at nonhomogeneous activation sites, we find $j_0 = 6 \times 10^{-4}$ to 2×10^{-2} A/cm^2.

Figure 4 shows a range of MoS_2/Pt_{20} current in red using the Butler–Volmer kinetic model of eqs 6 and 7 with the minimum/maximum j_0. We further compute the current of Pt(111) for comparison. Note that the Pt(111) surface is one of the most exposed termination on bulk Pt and is very stable in electrochemical conditions.[12−14] In ref 10, the current of the

https://dx.doi.org/10.1021/acs.chemmater.9b05244
Chem. Mater. 2020, 32, 1315−1321

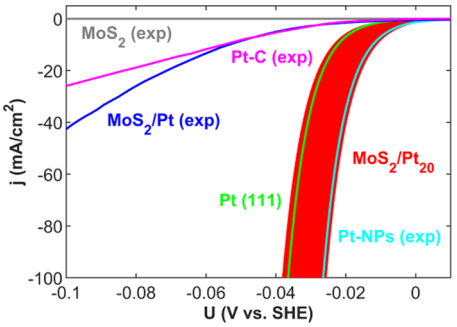

Figure 4. Exchange currents of MoS_2/Pt_{20} and Pt(111) computed from the Butler–Volmer kinetic model are compared with experimental results for MoS_2, Pt–C, and MoS_2/Pt NCs from ref 10 and for Pt NCs computed using j_0 from ref 22. The red shaded region corresponds to the currents of MoS_2/Pt_{20} computed by the upper/lower limit of j_0.

MoS_2-supported Pt cluster is smaller than our prediction for MoS_2/Pt_{20}. We believe that the origin of this discrepancy is due to the slow mass diffusion of H^+ onto the surface and solution impedance, which are well-known effects in catalysts with fast HER redox rates.[24] To validate this, we compute the Tafel slopes of Pt–C (commercial 10% Pt supported on activated charcoal) obtained from the same experimental setup and find the values of 40 and 300 mV/dec at 0 V and above −0.15 V, respectively.[10] These values are previously reported for Pt NCs without correcting for solution impendence and diffusion limits.[24] To further collaborate our arguments, we show in Figure 4 that our computed currents are in excellent agreement with the current of carbon-supported 2 nm Pt NCs, which was obtained after correction for H_2 diffusion and solution impedance.[22,26]

Finally, we discuss the potential role of MoS_2 in the catalytic activity of supported Pt NCs. Metal NCs are stabilized on MoS_2 due to metal–support interactions.[45−48] However, besides the beneficial role of MoS_2 in hindering NCs sintering and introducing new active sites at the MoS_2 edges, the substrate can also affect the activity of the metal cluster due to charge-transfer effects.[20,49,50] To investigate this, we examine an isolated Pt_{20} using a similar computational framework as done for MoS_2/Pt_{20}. To further aid in comparison, we keep the morphology of Pt_{20} as that of the supported one, although this configuration is clearly not optimum without the substrate. Also, we block hydrogen adsorption on the bottom surface of the Pt_{20} as it is in contact with MoS_2 for MoS_2/Pt_{20}. Figure S5 shows that the isotherm of the unsupported Pt_{20} is very similar to that of the supported MoS_2/Pt_{20} one. At the HER reversible potential, we obtain $\theta = 0.69$ with $\Delta G_H = -0.08$ eV for Pt_{20}, which is very close to $\theta = 0.60$ with $\Delta G_H = -0.08$ eV for MoS_2/Pt_{20}. Therefore, we conclude that the MoS_2 support does not have a significant effect on the catalytic activity of the Pt_{20} despite that the NCs adhere strongly to the support.[29] Indeed, this is also corroborated by noting that our results are in agreement with carbon-supported 2 nm Pt nanoparticles[22,26] that have weaker interactions with the substrates compared to those of MoS_2. The minimal impact of the substrate on the HER activity concluded in our study is in contrast to previous studies that showed that the HER activity of a single- or few-atom-supported metal clusters has a strong dependence on substrates.[3,51] This can be explained by the difference in the thickness of clusters; our study shows that only a single Pt layer can shield the support interactions with reactants. Hence, this makes our findings general for metal NCs with different shapes and sizes as well as for different substrates and different reactions.[52,53]

CONCLUSIONS

We have carried out first-principles calculations to understand the electrochemical hydrogen evolution reaction on MoS_2-supported platinum NCs. We use a cluster expansion method in conjunction with thermodynamic analysis to show that the HER adsorption free energy on MoS_2/Pt_{20} is comparable to that on Pt(111). We find that the preferred HER reaction pathway for MoS_2/Pt_{20} is the Volmer–Tafel pathway with the Volmer as the rate-determining step at the HER reversible potential, in agreement with experimental results for platinum electrodes. To best explain the experimental findings, we develop a kinetic Butler–Volmer model to study the voltammograms of Pt systems. We find that the current–potential characteristics of MoS_2/Pt_{20} with an exchange current density $\sim 6 \times 10^{-4}$–2×10^{-2} A/cm^2 are comparable to those of Pt(111) as well as the experimental results of Pt NCs. We also argue that the experimental HER currents on MoS_2-supported Pt NCs in ref 10 are underestimated due to solution impedance or diffusion limitations in electrochemical environments. Finally, we show that substrate interactions have no effect on the intrinsic HER activity of the NCs, which is different from the behaviors reported for single- or few-atom catalysts. The underpinning of this behavior is because the metal NCs with at least two layers of thickness would be exempted from the impact of substrates. Thus, our findings are general and applicable to NCs with different sizes and shapes on various supports as well as to different catalytic reactions.

ASSOCIATED CONTENT

Supporting Information

The Supporting Information is available free of charge at https://pubs.acs.org/doi/10.1021/acs.chemmater.9b05244.

Computational approach; details for derivation of eq 5; extrapolation scheme; results for unsupported NP; hydrogen diffusion on the NP; comparison in the HER activity between bulk Pt and supported Pt NCs (PDF)

AUTHOR INFORMATION

Corresponding Author

Wissam A. Saidi − *University of Pittsburgh, Pittsburgh, Pennsylvania;* orcid.org/0000-0001-6714-4832; Email: alsaidi@pitt.edu

Other Authors

Timothy T. Yang − *University of Pittsburgh, Pittsburgh, Pennsylvania*

Teck Leong Tan − *Institute of High-Performance Computing, Agency for Science, Technology and Research, Singapore, Singapore*

Complete contact information is available at: https://pubs.acs.org/10.1021/acs.chemmater.9b05244

Notes

The authors declare no competing financial interest.

https://dx.doi.org/10.1021/acs.chemmater.9b05244
Chem. Mater. 2020, 32, 1315−1321

■ ACKNOWLEDGMENTS

We acknowledge financial support from the National Science Foundation (Award No. DMR-1809085). We are grateful for computing time provided in part by the CRC resources at the University of Pittsburgh and Argonne Leadership Computing Facility, which is a DOE Office of Science User Facility supported under Contract DE-AC02-06CH11357.

■ REFERENCES

(1) Dresselhaus, M. S.; Thomas, I. L. Alternative energy technologies. *Nature* **2001**, *414*, 332.
(2) Parsons, R. The Rate of Electrolytic Hydrogen Evolution and the Heat of Adsorption of Hydrogen. *Trans. Faraday Soc.* **1958**, *54*, 1053−1063.
(3) Jiang, K.; Liu, B.; Luo, M.; Ning, S.; Peng, M.; Zhao, Y.; Lu, Y. R.; Chan, T. S.; de Groot, F. M. F.; Tan, Y. Single platinum atoms embedded in nanoporous cobalt selenide as electrocatalyst for accelerating hydrogen evolution reaction. *Nat. Commun.* **2019**, *10*, No. 1743.
(4) Zhang, H.; An, P.; Zhou, W.; Guan, B. Y.; Zhang, P.; Dong, J.; Lou, X. W. Dynamic traction of lattice-confined platinum atoms into mesoporous carbon matrix for hydrogen evolution reaction. *Sci. Adv.* **2018**, *4*, No. eaao6657.
(5) Zhang, J.; Zhao, Y.; Guo, X.; Chen, C.; Dong, C.-L.; Liu, R.-S.; Han, C.-P.; Li, Y.; Gogotsi, Y.; Wang, G. Single platinum atoms immobilized on an MXene as an efficient catalyst for the hydrogen evolution reaction. *Nat. Catal.* **2018**, *1*, 985−992.
(6) Grigoriev, S. A.; Millet, P.; Fateev, V. N. Evaluation of carbon-supported Pt and Pd nanoparticles for the hydrogen evolution reaction in PEM water electrolysers. *J. Power Sources* **2008**, *177*, 281−285.
(7) Cheng, N.; Stambula, S.; Wang, D.; Banis, M. N.; Liu, J.; Riese, A.; Xiao, B.; Li, R.; Sham, T. K.; Liu, L. M.; Botton, G. A.; Sun, X. Platinum single-atom and cluster catalysis of the hydrogen evolution reaction. *Nat. Commun.* **2016**, *7*, No. 13638.
(8) Proch, S.; Wirth, M.; White, H. S.; Anderson, S. L. Strong effects of cluster size and air exposure on oxygen reduction and carbon oxidation electrocatalysis by size-selected Pt(n) (n </= 11) on glassy carbon electrodes. *J. Am. Chem. Soc.* **2013**, *135*, 3073−86.
(9) Tsunoyama, H.; Yamano, Y.; Zhang, C.; Komori, M.; Eguchi, T.; Nakajima, A. Size-Effect on Electrochemical Hydrogen Evolution Reaction by SingleSize Platinum Nanocluster Catalysts Immobilized on Strontium Titanate. *Top. Catal.* **2018**, *61*, 126−135.
(10) Huang, X.; Zeng, Z.; Bao, S.; Wang, M.; Qi, X.; Fan, Z.; Zhang, H. Solution-phase epitaxial growth of noble metal nanostructures on dispersible single-layer molybdenum disulfide nanosheets. *Nat. Commun.* **2013**, *4*, No. 1444.
(11) Skúlason, E.; Karlberg, G. S.; Rossmeisl, J.; Bligaard, T.; Greeley, J.; Jónsson, H.; Nørskov, J. K. Density functional theory calculations for the hydrogen evolution reaction in an electrochemical double layer on the Pt(111) electrode. *Phys. Chem. Chem. Phys.* **2007**, *9*, 3241−3250.
(12) Liao, H.-G.; Zherebetskyy, D.; Xin, H.; Czarnik, C.; Ercius, P.; Elmlund, H.; Pan, M.; Wang, L.-W.; Zheng, H., Facet development during platinum nanocube growth. *Science* **2014**, *345* ().
(13) McCrum, I. T.; Hickner, M. A.; Janik, M. J. First-Principles Calculation of Pt Surface Energies in an Electrochemical Environment: Thermodynamic Driving Forces for Surface Faceting and Nanoparticle Reconstruction. *Langmuir* **2017**, *33*, 7043−7052.
(14) Conway, B. E.; Tilak, B. V. Interfacial processes involving electrocatalytic evolution and oxidation of H2, and the role of chemisorbed H. *Electrochim. Acta* **2002**, *47*, 3571−3594.
(15) Gomez, R.; Fernandez-Vega, A.; Feliu, J. M.; Aldaz, A. Hydrogen evolution on platinum single crystal surfaces: effects of irreversibly adsorbed bismuth and antimony on hydrogen adsorption and evolution on platinum (100). *J. Phys. Chem. A* **1993**, *97*, 4769−4776.
(16) Tan, T. L.; Wang, L.-L.; Zhang, J.; Johnson, D. D.; Bai, K. Platinum Nanoparticle During Electrochemical Hydrogen Evolution: Adsorbate Distribution, Active Reaction Species, and Size Effect. *ACS Catal.* **2015**, *5*, 2376−2383.
(17) Zalitis, C. M.; Kucernak, A. R.; Sharman, J.; Wright, E. Design principles for platinum nanoparticles catalysing electrochemical hydrogen evolution and oxidation reactions: edges are much more active than facets. *J. Mater. Chem. A* **2017**, *5*, 23328−23338.
(18) Wei, G. F.; Liu, Z. P. Restructuring and Hydrogen Evolution on Pt Nanoparticle. *Chem. Sci.* **2015**, *6*, 1485−1490.
(19) Voiry, D.; Salehi, M.; Silva, R.; Fujita, T.; Chen, M.; Asefa, T.; Shenoy, V. B.; Eda, G.; Chhowalla, M. Conducting MoS(2) nanosheets as catalysts for hydrogen evolution reaction. *Nano Lett.* **2013**, *13*, 6222−7.
(20) Tsai, C.; Abild-Pedersen, F.; Nørskov, J. K. Tuning the MoS2 Edge-Site Activity for Hydrogen Evolution via Support Interactions. *Nano Lett.* **2014**, *14*, 1381−1387.
(21) Zhou, M.; Bao, S.; Bard, A. J. Probing Size and Substrate Effects on the Hydrogen Evolution Reaction by Single Isolated Pt Atoms, Atomic Clusters, and Nanoparticles. *J. Am. Chem. Soc.* **2019**, *141*, 7327−7332.
(22) Durst, J.; Simon, C.; Hasché, F.; Gasteiger, H. A. Hydrogen Oxidation and Evolution Reaction Kinetics on Carbon Supported Pt, Ir, Rh, and Pd Electrocatalysts in Acidic Media. *J. Electrochem. Soc.* **2015**, *162*, F190−F203.
(23) Sheng, W.; Gasteiger, H. A.; Shao-Horn, Y. Hydrogen Oxidation and Evolution Reaction Kinetics on Platinum: Acid vs Alkaline Electrolytes. *J. Electrochem. Soc.* **2010**, *157*, B1529−B1536.
(24) Zheng, J.; Yan, Y.; Xu, B. Correcting the Hydrogen Diffusion Limitation in Rotating Disk Electrode Measurements of Hydrogen Evolution Reaction Kinetics. *J. Electrochem. Soc.* **2015**, *162*, F1470−F1481.
(25) Nørskov, J. K.; Bligaard, T.; Logadottir, A.; Kitchin, J. R.; Chen, J. G.; Pandelov, S.; Stimming, U. Trends in the Exchange Current for Hydrogen Evolution. *J. Electrochem. Soc.* **2005**, *152*, J23−J26.
(26) Kibsgaard, J.; Jaramillo, T. F. Molybdenum phosphosulfide: an active, acid-stable, earth-abundant catalyst for the hydrogen evolution reaction. *Angew. Chem., Int. Ed.* **2014**, *53*, 14433−7.
(27) VandeVondele, J.; Krack, M.; Mohamed, F.; Parrinello, M.; Chassaing, T.; Hutter, J. Quickstep: Fast and accurate density functional calculations using a mixed Gaussian and plane waves approach. *Comput. Phys. Commun.* **2005**, *167*, 103−128.
(28) Perdew, J. P.; Burke, K.; Ernzerhof, M. Generalized Gradient Approximation Made Simple. *Phys. Rev. Lett.* **1996**, *77*, 3865−3868.
(29) Shi, Y.; Song, B.; Shahbazian-Yassar, R.; Zhao, J.; Saidi, W. A. Experimentally Validated Structures of Supported Metal Nanoclusters on MoS2. *J. Phys. Chem. Lett.* **2018**, *9*, 2972−2978.
(30) Zarkevich, N. A.; Tan, T. L.; Johnson, D. D. First-principles prediction of phase-segregating alloy phase diagrams and a rapid design estimate of their transition temperatures. *Phys. Rev. B: Condens. Matter Mater. Phys.* **2007**, *75*, No. 104203.
(31) Zarkevich, N. A.; Tan, T. L.; Wang, L. L.; Johnson, D. D. Low-energy antiphase boundaries, degenerate superstructures, and phase stability in frustrated fcc Ising model and Ag-Au alloys. *Phys. Rev. B: Condens. Matter Mater. Phys.* **2008**, *77*, No. 144208.
(32) Tsai, C.; Li, H.; Park, S.; Park, J.; Han, H. S.; Norskov, J. K.; Zheng, X.; Abild-Pedersen, F. Electrochemical generation of sulfur vacancies in the basal plane of MoS2 for hydrogen evolution. *Nat. Commun.* **2017**, *8*, No. 15113.
(33) Li, H.; Tsai, C.; Koh, A. L.; Cai, L.; Contryman, A. W.; Fragapane, A. H.; Zhao, J.; Han, H. S.; Manoharan, H. C.; Abild-Pedersen, F.; Norskov, J. K.; Zheng, X. Activating and optimizing MoS2 basal planes for hydrogen evolution through the formation of strained sulphur vacancies. *Nat. Mater.* **2016**, *15*, 48−53.
(34) Skúlason, E.; Tripkovic, V.; Björketun, M. E.; Gudmundsdóttir, S.; Karlberg, G.; Rossmeisl, J.; Bligaard, T.; Jónsson, H.; Nørskov, J. K. Modeling the Electrochemical Hydrogen Oxidation and Evolution Reactions on the Basis of Density Functional Theory Calculations. *J. Phys. Chem. C* **2010**, *114*, 18182−18197.

(35) Gnanasekar, P.; Periyanagounder, D.; Kulandaivel, J. Vertically aligned MoS2 nanosheets on graphene for highly stable electrocatalytic hydrogen evolution reactions. *Nanoscale* **2019**, *11*, 2439−2446.
(36) Yang, T. T.; Saidi, W. A. Tuning the hydrogen evolution activity of β-Mo2C nanoparticles via control of their growth conditions. *Nanoscale* **2017**, *9*, 3252−3260.
(37) Chase, M. W., Jr. NIST-JANAF Themochemical Tables, Fourth Edition. *J. Phys. Chem. Ref. Data Monograph* **1998**, 1−1951.
(38) Saidi, W. A. Oxygen Reduction Electrocatalysis Using N-Doped Graphene Quantum-Dots. *J. Phys. Chem. Lett.* **2013**, *4*, 4160−4165.
(39) Rossmeisl, J.; Skúlason, E.; Björketun, M. E.; Tripkovic, V.; Nørskov, J. K. Modeling the electrified solid−liquid interface. *Chem. Phys. Lett.* **2008**, *466*, 68−71.
(40) Chan, K.; Nørskov, J. K. Potential Dependence of Electrochemical Barriers from ab Initio Calculations. *J. Phys. Chem. Lett.* **2016**, *7*, 1686−1690.
(41) Watzele, S.; Fichtner, J.; Garlyyev, B.; Schwämmlein, J. N.; Bandarenka, A. S. On the Dominating Mechanism of the Hydrogen Evolution Reaction at Polycrystalline Pt Electrodes in Acidic Media. *ACS Catal.* **2018**, *8*, 9456−9462.
(42) Sheng, W.; Zhuang, Z.; Gao, M.; Zheng, J.; Chen, J. G.; Yan, Y. Correlating hydrogen oxidation and evolution activity on platinum at different pH with measured hydrogen binding energy. *Nat. Commun.* **2015**, *6*, No. 5848.
(43) Elbert, K.; Hu, J.; Ma, Z.; Zhang, Y.; Chen, G.; An, W.; Liu, P.; Isaacs, H. S.; Adzic, R. R.; Wang, J. X. Elucidating Hydrogen Oxidation/Evolution Kinetics in Base and Acid by Enhanced Activities at the Optimized Pt Shell Thickness on the Ru Core. *ACS Catal.* **2015**, *5*, 6764−6772.
(44) Zheng, J.; Sheng, W.; Zhuang, Z.; Xu, B.; Yan, Y. Universal dependence of hydrogen oxidation and evolution reaction activity of platinum-group metals on pH and hydrogen binding energy. *Sci. Adv.* **2016**, *2*, No. e1501602.
(45) Saidi, W. A. Trends in the Adsorption and Growth Morphology of Metals on the MoS2(001) Surface. *Cryst. Growth Des.* **2015**, *15*, 3190−3200.
(46) Saidi, W. A. Density Functional Theory Study of Nucleation and Growth of Pt Nanoparticles on MoS2(001) Surface. *Cryst. Growth Des.* **2015**, *15*, 642−652.
(47) Song, B.; He, K.; Yuan, Y.; Sharifi-Asl, S.; Cheng, M.; Lu, J.; Saidi, W. A.; Shahbazian-Yassar, R. In situ study of nucleation and growth dynamics of Au nanoparticles on MoS2 nanoflakes. *Nanoscale* **2018**, *10*, 15809−15818.
(48) Saidi, W. A. Influence of strain and metal thickness on metal-MoS2 contacts. *J. Chem. Phys.* **2014**, *141*, No. 094707.
(49) Behranginia, A.; Asadi, M.; Liu, C.; Yasaei, P.; Kumar, B.; Phillips, P.; Foroozan, T.; Waranius, J. C.; Kim, K.; Abiade, J.; Klie, R. F.; Curtiss, L. A.; Salehi-Khojin, A. Highly Efficient Hydrogen Evolution Reaction Using Crystalline Layered Three-Dimensional Molybdenum Disulfides Grown on Graphene Film. *Chem. Mater.* **2016**, *28*, 549−555.
(50) Chatti, M.; Gengenbach, T.; King, R.; Spiccia, L.; Simonov, A. N. Vertically Aligned Interlayer Expanded MoS2 Nanosheets on a Carbon Support for Hydrogen Evolution Electrocatalysis. *Chem. Mater.* **2017**, *29*, 3092−3099.
(51) Wang, D.; Li, Q.; Han, C.; Xing, Z.; Yang, X. Single-atom ruthenium based catalyst for enhanced hydrogen evolution. *Appl. Catal., B* **2019**, *249*, 91−97.
(52) Li, J. S.; Wang, Y.; Liu, C. H.; Li, S. L.; Wang, Y. G.; Dong, L. Z.; Dai, Z. H.; Li, Y. F.; Lan, Y. Q. Coupled molybdenum carbide and reduced graphene oxide electrocatalysts for efficient hydrogen evolution. *Nat. Commun.* **2016**, *7*, No. 11204.
(53) Ojani, R.; Valiollahi, R.; Raoof, J.-B. Comparison between graphene supported Pt hollow nanospheres and graphene supported Pt solid nanoparticles for hydrogen evolution reaction. *Energy* **2014**, *74*, 871−876.

https://dx.doi.org/10.1021/acs.chemmater.9b05244
Chem. Mater. 2020, 32, 1315−1321